European Biophysics Journal (2021) 50:513–521
https://doi.org/10.1007/s00249-021-01538-0

ORIGINAL ARTICLE

Dps–DNA interaction in *Marinobacter hydrocarbonoclasticus* protein: effect of a single-charge alteration

João P. Jacinto[1] · Daniela Penas[1] · João P. L. Guerra[1] · Ana V. Almeida[1] · Nykola C. Jones[2] · Søren V. Hoffmann[2] · Pedro Tavares[1] · Alice S. Pereira[1]

Received: 2 October 2020 / Revised: 6 April 2021 / Accepted: 14 April 2021 / Published online: 26 April 2021

Abstract

DNA-binding proteins from starved cells (Dps) are members of the ferritin family of proteins found in prokaryotes, with hollow rounded cube-like structures, composed of 12 equal subunits. These protein nanocages are bifunctional enzymes that protect the cell from the harmful reaction of iron and peroxide (Fenton reaction), thus preventing DNA damage by oxidative stress. Ferrous ions are oxidized at specific iron-binding sites in the presence of the oxidant and stored in its cavity that can accommodate up to ca. 500 iron atoms. DNA-binding properties of Dps are associated with the N-terminal, positive charge rich, extensions that can promote DNA binding and condensation, apparently by a cooperative binding mechanism. Here, we describe the binding and protection activities of *Marinobacter hydrocarbonoclasticus* Dps using Electrophoretic Mobility Shift Essays (EMSA), and synchrotron radiation circular dichroism (SRCD) spectroscopy. While no DNA condensation was observed in the tested conditions, it was possible to determine a Dps–DNA complex formation with an apparent dissociation constant of 6.0 ± 1.0 μM and a Hill coefficient of 1.2 ± 0.1. This interaction is suppressed by the inclusion of a single negative charge in the N-terminal region by point mutation. In Dps proteins containing a ferric mineral core (above 96 Fe/protein), DNA binding was impaired. SRCD data clearly showed that no significant modification existed either in secondary structure or protein stability of WT, Q14E variant and core containing proteins. It was, however, interesting to note that, in our experimental conditions, thermal denaturation induced protein aggregation that caused artifacts in thermal denaturation curves, which were dependent on radiation flux and vertical arrangement of the CD cell.

Keywords DNA-binding protein from starved cells · Protein nanocages · Thermal stability · Synchrotron radiation circular dichroism

Introduction

Natural protein cages are profuse, including virus-like particle (VLP), chaperones, heat shock proteins and ferritins, among others, fulfilling a diversity of functions (Heddle et al. 2017; Aumiller et al. 2018). Dps (DNA-binding proteins from starved cells), one of the smallest protein cages, are homopolymers belonging to the ferritin family involved in the cellular response to multiple stresses (oxidative, thermal, UV and extreme pH) during the stationary phase (Nair and Finkel 2004; Karas et al. 2015). It is able to form crystalline DNA–protein complexes to adapt to unfavorable conditions (Wolf et al. 1999). Their hollow rounded cube-like structure is composed of 12 subunits, folded into 4-helix bundles (each monomer has an additional small helix) (Zhang and Orner 2011; Theil et al. 2016). The Dps cage has an outer diameter of approximately 8–9 nm and

João P. Jacinto and Daniela Penas have contributed equally to this work.

Special Issue: COST Action CA15126, MOBIEU: Between atom and cell.

✉ Alice S. Pereira
masp@fct.unl.pt

[1] Molecular Biophysics Laboratory, UCIBIO, Departamento de Química, Faculdade de Ciências e Tecnologia, Universidade NOVA de Lisboa, 2829-516 Caparica, Portugal

[2] ISA, Department of Physics and Astronomy, Aarhus University, 8000 Aarhus C, Denmark

an inner cavity of 4–5 nm, which can accommodate up to ∽ 500 ferric ions (Haikarainen and Papageorgiou 2010). In most proteins, the inner cavity is connected to the exterior through two types of channels, a threefold symmetric channel formed by the junction of N-terminal tails (similar to the ferritin ones and thus designated ferritin-like channels) and a second type created by the C-terminus of monomers (due to its uniqueness, these were termed Dps-like channels) (Crichton and Declercq 2010; Calhoun and Kwon 2011). Iron traffic to and from the cavity occurs through the negatively charged ferritin-like channels directed by electrostatic fields (Crichton and Declercq 2010).

The main function of Dps is iron detoxification, rather than iron storage. Sequestration of ferrous iron minimizes the formation of iron-mediated reactive oxidative species by Fenton reactions and, thus, cell damage. To fulfill this function Dps proteins contain unique ferroxidase sites located at the interface between two anti-parallel subunits (two ferroxidase sites per dimer, ∽ 2 nm apart, in a total of 12 sites), where ferrous ions are rapidly oxidized to the ferric state. The ferroxidase site is believed to be binuclear, with two non-equivalent iron-binding sites, where two ferrous ions are converted into ferric species with reduction of one molecule of hydrogen peroxide (H_2O_2) (Ilari et al. 2000; Paszko and Senge 2012). Molecular oxygen can also oxidize ferrous ions, but at a much slower rate when compared with the co-substrate H_2O_2. Once oxidized, the ferric-oxo species are translocated to the cavity for mineral formation (biomineralization reaction) (Pesek et al. 2011).

While all Dps are able to sequester Fe^{2+} ions, oxidize and store them in the ferric mineral form, not all have the capacity to bind DNA. Some can interact with DNA (supercoiled or linear plasmid or genomic DNA) without sequence specificity, protecting it from chemical and physical damage. In the cell, Dps proteins condense DNA in the stationary phase, allowing for DNA protection against mechanical stress and enzymatic degradation (Zeth 2012; Hitchings et al. 2014). The DNA-binding activity of Dps has been the motive for intensive debate in the scientific community. Given the fact that both DNA and Dps surfaces are negatively charged it has been proposed that the positively charged residues, variable in number, at the N- or C-terminal tails are responsible for DNA binding (Stillman et al. 2005; Andrews 2010; Hitchings et al. 2014). In a few cases, as in *Helicobacter* (*H.*) *pylori* Dps (also known as neutrophil-activating protein), the polyanion DNA molecule interacts with the positive surface of the protein (Ceci et al. 2007).

Dps proteins that condense DNA have a positive (presence of lysine and/or arginine residues) and protruding N- or C-terminal extensions (Crichton 2002; Andrews 2010). The absence of a protruding mobile tail nullifies the condensation activity. It has been shown that in the *Escherichia* (*E.*) *coli* Dps, the interaction with DNA occurs due to three lysine residues in the mobile N-terminal extension, that interact with the phosphate groups on DNA (Grant et al. 1998). Deletion of 2 or all 3 lysine residues impairs the DNA condensation activity in the first case and abolishes DNA binding in the second (Chiancone and Ceci 2010).

The requirement of a flexible N-terminal extension, besides multiple positive residues, for DNA binding and condensation was demonstrated for the *Agrobacterium fabrum* (formerly *Agrobacterium tumefaciens*) Dps. Despite the presence of 3 lysine residues in the N-terminal region, this protein, contrarily to the *E. coli* one, is unable to bind DNA because the N-terminal regions are immobilized through weak interactions to the dodecamer surface, namely hydrogen bond and electrostatic interactions (Ceci et al. 2003). Contrasting with other prokaryotic nucleoid-associated proteins or eukaryotic histones, binding of Dps to DNA does not affect the initiation of transcription and slightly alters the transcriptome of the *E. coli* stationary phase, but blocks the activity of endonucleases, in vitro (Janissen et al. 2018).

With this work, we aim to elucidate the role of the N-terminal extension of Dps from *Marinobacter hydrocarbonoclasticus* on DNA-binding activity and protection. Apo and holo forms of wild-type (WT) Dps and variant (Q14E), wherein a single negative charge was placed on the N-terminal region, were incubated with a supercoiled plasmid, pUC19, and complex formation was studied by Electrophoretic Mobility Shift Assays (EMSAs).

DNA protection tests against hydroxyl radicals and proteolytic hydrolysis were also conducted. The secondary structure of wild-type Dps, apo and holo forms, and Q14E variant proteins was assessed by synchrotron radiation circular dichroism (SRCD), in the absence or presence of pUC19 plasmid DNA. Importantly, the use of a horizontally oriented sample holder in a non-conventional CD setup, denoted the periscope chamber, is described to properly study the thermal stability of the protein.

Results and discussion

DNA binding

The DNA-binding capacity of the apo form (iron free) of *M. hydrocarbonoclasticus* Dps-WT protein was evaluated by EMSA (Fig. 1). The results showed that the protein was able to bind to supercoiled plasmid pUC19. Binding of Dps-WT to pUC19 produced larger protein–DNA complexes which migrated slower than the free form of supercoiled pUC19 (Fig. 1a, lanes 3–13). In the conditions tested, the intensity of the complex band increased with protein concentration, with an apparent saturation at around 10 μM Dps-WT. The observed binding was specific for Dps-WT, since substitution with BSA (a protein that does not bind

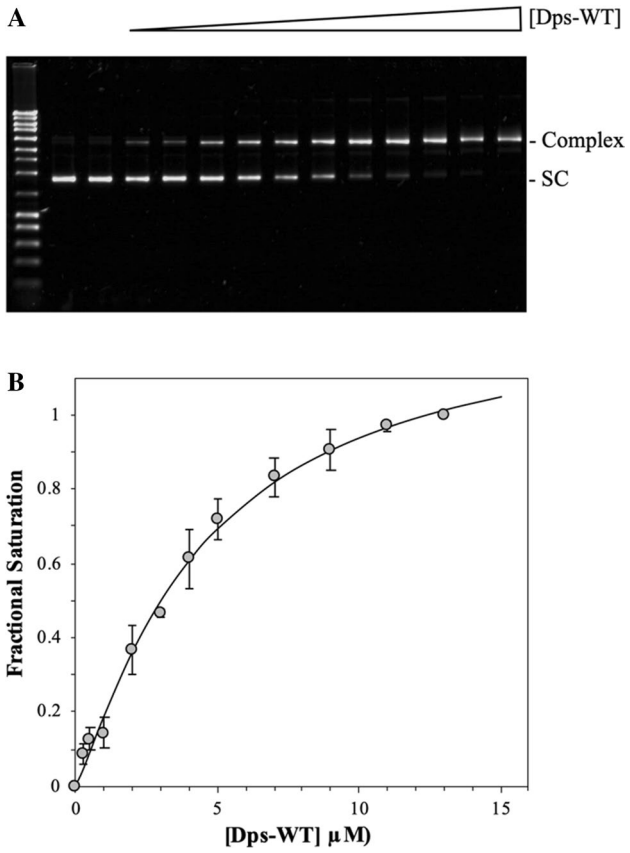

Fig. 1 Binding of *M. hydrocarbonoclasticus* Dps-WT to supercoiled plasmid pUC19 in 50 mM MOPS buffer pH 7.0, 50 mM NaCl, analyzed by EMSA. **a** EMSA on 1% agarose gel. 1—supercoiled plasmid pUC19 (10 nM); 2—binding reaction of BSA (3 µM) to supercoiled pUC19 (10 nM); 3–13—binding of Dps-WT (0.25, 0.50, 1.0, 2.0, 3.0, 4.0, 5.0, 7.0, 9.0, 11 and 13 µM) to supercoiled pUC19 (10 nM). M—NZYLadder III. The free supercoiled plasmid pUC19 band (SC) and the pUC19-protein complex band (Complex) are identified on the right. **b** Hill plot of DNA binding by Dps-WT from four sets of EMSA experiments using increasing concentrations of protein (between 0.25 and 13 µM) and supercoiled plasmid pUC19 (10 nM). Less than 8% uncertainty is estimated for the fractional saturation

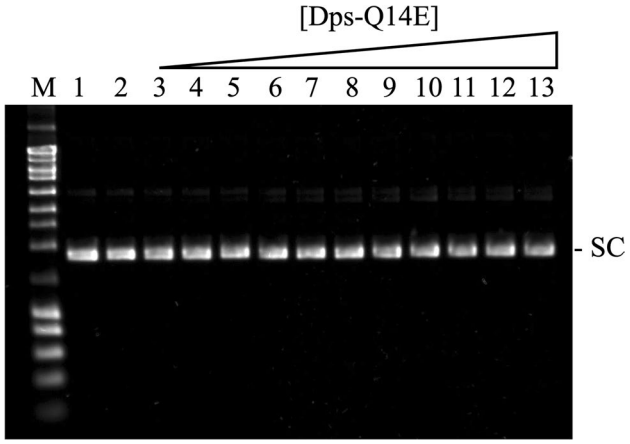

Fig. 2 EMSA of the binding reaction of variant Dps-Q14E with supercoiled plasmid pUC19 in 50 mM MOPS buffer pH 7.0, 50 mM NaCl. 1—supercoiled plasmid pUC19 (10 nM); 2—binding reaction of BSA (3 µM) to supercoiled pUC19 (10 nM); 3–13—binding of Dps-WT (0.25, 0.50, 1.0, 2.0, 3.0, 4.0, 5.0, 7.0, 9.0, 11 and 13 µM) to supercoiled pUC19 (10 nM). M—NZYLadder III. The free supercoiled plasmid pUC19 band (SC) is indicated

DNA) did not show any shift of the free form of supercoiled pUC19 (Fig. 1a, lane 2). The fractional complex formation was plotted as a function of protein concentration and fitted with the Hill equation (Fig. 1b). In our experimental conditions, we calculated an apparent dissociation constant, K_D of 6.0 ± 1 µM and a Hill coefficient, n of 1.2 ± 0.1. The Hill coefficient indicates a moderate positive cooperativity on DNA binding and is comparable with the values reported in the literature for the binding of *Deinococcus radiodurans* Dps-1 to a 26-bp DNA duplex (n of 1.3 ± 0.2) or to the binding of *Desulfovibrio vulgaris* Dps-like bacterioferritin to a supercoiled plasmid DNA (n = 1.3 ± 0.2) (Timóteo et al. 2012; Nguyen et al. 2012). In turn, the K_D value obtained for *M. hydrocarbonoclasticus* Dps is similar to the one reported for *H. pylori* Dps binding to a linearized long plasmid DNA (3100 bp) (Ceci et al. 2007). It has been reported that most DNA–Dps interactions are mediated by a mobile N- or C-terminal extension, dependent on the presence of positively charged residues (lysines and/or arginines) (Ceci 2004; Haikarainen and Papageorgiou 2010; Calhoun and Kwon 2011).

The N-terminal tail of *M. hydrocarbonoclasticus* Dps (MGKNFIGLDTDKTQK) contains three lysine residues positively charged at pH 7.0, that can establish electrostatic interactions with DNA. In the experimental conditions tested, *M. hydrocarbonoclasticus* Dps did not promote condensation of the DNA. The presence of a single sharp band and the electrophoretic migration of the complex band suggest that *M. hydrocarbonoclasticus* Dps binds to supercoiled circular DNA changing its topology to a more relaxed form. Other Dps proteins are unable to condense DNA, namely the Dps-1 from *Mycobacterium smegmatis*, Dps from *Mycobacterium abscessus* subsp. *massiliense* and Dps-4 and Dps-5 from the cyanobacterium *Nostoc punctiforme* (Ceci et al. 2007; Moparthi et al. 2019; de Alcântara et al. 2020). This behavior was attributed to the presence of four negatively charged amino acid residues in the C-terminal extension that would compensate (or partly compensate) the five positively charged ones. This could explain the inability of *M. hydrocarbonoclasticus* Dps of DNA condensation, since 3 lysines and 2 aspartate residues are present on its N-terminal extension, composed of 15 amino acid residues. To probe the effect of negatively charged residues on the N-terminal extension, a variant was prepared, replacing glutamine-14 by a glutamate residue, adding a negative charge at pH 7.0. The EMSA gel is presented in Fig. 2. It is clear that

Dps-Q14E variant was not able to bind DNA, demonstrating that a single-charge residue substitution was enough to alter the binding affinity of the protein towards the DNA. In fact, the mutation resulted in a substantial decrease of the pI of the first 15 residue fragment, from 8.25 for the wild type to 5.88 for the Q14E variant. Alternatively, the non-condensation capacity of *M. hydrocarbonoclasticus* Dps could be due to the fact that it does not self-aggregate. Effectively, the ability of *E. coli* Dps of forming large DNA–Dps complexes and DNA condensation has been attributed to its self-aggregation propensity (Ceci 2004). To investigate the affinity for DNA of iron-loaded Dps protein, samples of holo protein were prepared with different amounts of ferric mineral core inside its inner cavity, using H_2O_2 or O_2 as co-substrate. The DNA-binding capacity of the holo protein was assessed by EMSA. Figure 3 shows that the iron-loaded (holo) forms have lower affinity to DNA than the apo Dps (iron-free), decaying with higher iron loads. When the protein was loaded with substoichiometric amounts of Fe^{2+} ions (relative to the putative iron binding sites), between 12 and 48 Fe^{2+}/protein, some complex was still observed

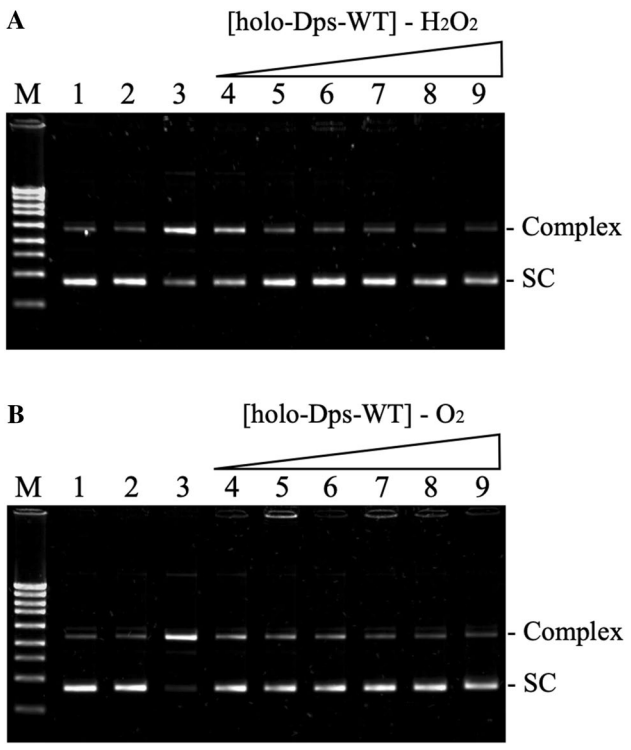

Fig. 3 DNA-binding analysis of iron-loaded Dps in 50 mM MOPS buffer pH 7.0, 50 mM NaCl. Binding reaction with iron loaded (holo) Dps-WT produced in the presence of H_2O_2 (**a**) and O_2 (**b**). 1—plasmid pUC19 (10 nM); 2—binding reaction of BSA (3 µM) to plasmid pUC19 (10 nM); 3—binding control of apo-Dps-WT (13 µM) to plasmid pUC19 (10 nM); 4–9—binding of Dps-WT loaded with 12, 24, 48, 96, 192 and 384 Fe^{2+}/protein; M— NZYLadder III. The free supercoiled plasmid band (SC) and the protein–DNA band (complex) are indicated on the right

(lanes 4–6 in gels in Figure 3), that had become non-significant for proteins with iron loads above 48. This observation had led us to suggest that when the iron was mainly in the mineral core form (ferric mineral in the protein inner cavity) (Penas et al. 2019), the protein no longer has the ability to bind DNA. Tosha and colleagues have proposed a role for the N-terminal extensions of M ferritin from frog, a maxi-ferritin composed of 24 subunits (Tosha et al. 2012). According to the authors, the N-terminal extensions would function as pore gates for ferrous ions entry/exit to/from the protein inner cavity through the ferritin-like channels. The pore gates would participate in a network of interactions (hydrogen bonds and salt bridges), involving residues Q6 and N7 (frog M ferritin numbering) from the N-terminal, R72 (in helix 2) and R122 (from the loop between helices 2 and 3), conserved in all eukaryotic ferritins. Although these residues are absent in Dps, both types of ferritins share the same 3-fold symmetry channel, the so-called ferritin-like channels, and possess protruding N-terminal extensions. As mentioned before, the channels create an electrostatic potential, due to the presence of negatively charged residues (aspartates and glutamates) that direct the Fe^{2+} ions traffic to and from the protein cavity, down electrochemical gradient (Crichton and Declercq 2010). While absent in some Dps, we can envisage a similar role for amino acid residues N4 and Q13 in the N-terminal extension *of M. hydrocarbonoclasticus* Dps, gating the ferritin-like channels. In the presence of a ferric mineral core inside the protein, subtle structural changes would occur at the channel gate (closing the gate to avoid leakage of Fe^{2+} ions) inhibiting DNA binding, allowing the protein to act as an iron storage enzyme.

Nevertheless, binding of Dps to DNA seems to occur in different typologies, depending on the protein and microorganism. Although the most common mechanism involves the positive N- or C-terminal extensions or surfaces, the requirement of ferrous ions and H_2O_2, has also been described. In the case of Dps from *Campylobacter jejuni*, DNA binding seems to be induced by the presence of Fe^{2+} ions or H_2O_2 (Huergo et al. 2013).

Assessing the secondary structure of proteins and DNA–Dps complex

SRCD was used to evaluate if the Q14E point mutation and the presence of a mineral core in the wild-type protein inner cavity (holo form with 96 Fe/Dps protein), affected DNA binding by altering the secondary structure of *M. hydrocarbonoclasticus* Dps.

SRCD spectra are presented in Fig. 4 and are consistent with proteins with a high content of α-helices as expected from the crystallographic structures of homologs. It should be noted that SRCD data is significant because it can reveal subtle changes in protein secondary structure. This is due to

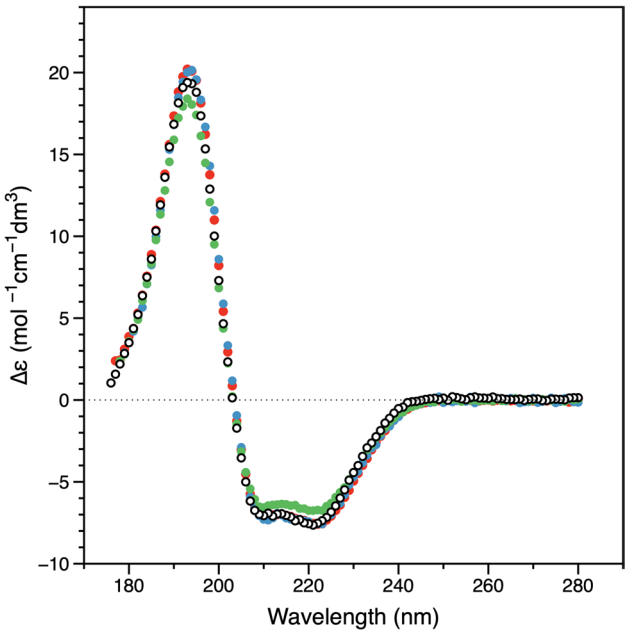

Fig. 4 SRCD spectra obtained at 25 °C for apo Dps-WT (white circles); Dps-Q14E variant (red circles); Holo form with 96 Fe/Dps-WT protein (blue circles) and Dps-WT (4 μM) incubated with supercoiled pUC19 (125 nM) (green circles)

the high energies and photon flux achieved by the synchrotron beam, which makes possible the use of an extended spectral range from 175 to 195 nm when compared to conventional benchtop spectrometers. Table 1 shows the calculated secondary structures percentages for each sample (see Figure S1 in ESI for the theoretical fits of each spectrum). Data obtained for the apo (Fig. 4, white circles) and holo forms of Dps-WT (Fig. 4, blue circles) showed that the presence of 96 Fe/Dps mineral core did not induce any significant differences at the secondary structure level (displaying a slight increase in α-helices). The Dps-Q14E variant (Fig. 4, red circles) also maintained the structural features of Dps-WT. A more significant difference was observed for the protein incubated with pUC19 (Fig. 4, green circles), where spectral analysis showed a reduction of 10% in α-helices and an increase of 6% of unordered component. This suggests a more flexible structure in agreement with the rationale leading to the formation of DNA–Dps complex observed in the EMSA experiments described above.

Table 1 Calculated secondary structures percentages obtained by analysis with Dichroweb online server

Secondary structure (%)	Sample			
	Dps-WT	Dps-Q14E	Dps-WT holo form	Dps-WT + pUC19
Regular helix	55	57	58	47
Distorted helix	23	24	24	20
Regular strand	5	4	5	7
Distorted strand	1	1	0	3
Turns	7	6	5	8
Unordered	9	8	8	15

Thermal stability was probed for all protein forms, with similar results being obtained. The data obtained for Dps-WT displayed a characteristic behavior observed for all tested samples and will be used here as an example of such peculiar behavior. Comparable temperature scans between 5 and 90 °C were obtained for different experimental setups and as shown in Fig. 5A, the denaturation profile was setup dependent. In both SRCD datasets acquired using the standard dual Peltier chamber (Figure 5, green circles) and the Chirascan standard chamber (Fig. 5, orange circles), an inflexion around 40–45 °C was noticeable, albeit with differences in the overall profile. Such inflexions were not observed in SRCD data acquired with the periscope chamber, which clearly suggests aggregation leading to precipitation of protein samples. To corroborate this conclusion, DLS temperature dependence data were obtained for the same protein/buffer system. Fig. 5b revealed that the Z-average size abruptly increases at approximately 40 °C, supporting the aggregation behavior inferred from

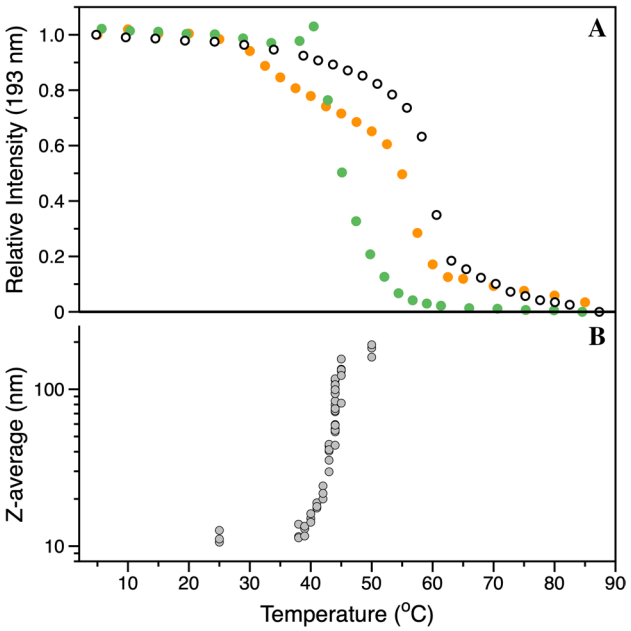

Fig. 5 Thermal denaturation studies of Dps-WT protein (**a**). Data was obtained using SRCD with periscope chamber (white circles); CD with a Chirascan standard chamber (orange circles); and SRCD with standard dual Peltier chamber (green circles). Thermal denaturation curves are derived from signal intensity at 193 nm versus temperature with proper baseline subtraction and normalization. **b** shows the Z-average size calculated from raw DLS data as a function of temperature

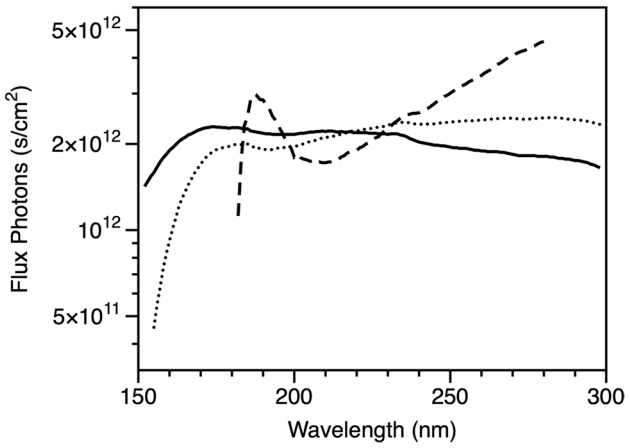

Fig. 6 Photon flux measurements for the SRCD and CD setups used. Data were obtained using standard dual Peltier chamber (solid line) periscope chamber (dotted line); and Chirascan standard chamber (dashed line)

Table 2 Beam size dimensions of used circular dichroism setups

Beam size	Synchrotron radiation		Benchtop
	Standard dual Peltier chamber	Periscope chamber	Chirascan standard chamber
Width (mm)	3.5	4	8
Height (mm)	5	4.5	11
Area (mm^2)	17.5	18	88

the multiple SRCD and CD data. SRCD results obtained with the periscope chamber setup also showed that no loss (or little loss) of α-helical structure occurred upon aggregation and that the thermal denaturation was better described by a T_m temperature of ~ 60 °C. The results presented here demonstrate the importance of a horizontal mounting position such as the one used in the periscope chamber setup. More, if unaware, the possibility exists to extract misleading information about structural thermal stability from circular dichroism data. To try to explain differences in the curves obtained using the standard dual Peltier chamber and the Chirascan standard chamber, beam sizes and photon flux were measured for all used setups (Fig. 6). As expected, photon flux below 185 nm was different for synchrotron beam-based setups and the Chirascan setup, but no significant differences were observed in less energetic wavelengths (up until 250 nm). Beam size measurements showed that the synchrotron beam-based setups have a significantly smaller area than the benchtop spectrometer used (Table 2). In fact, in the benchtop spectrometer, the beam size on the sample is almost 5x that for the synchrotron radiation facility, thus explaining the different profiles observed, created by aggregation (and precipitation) displacement effects in the cell.

Protection assays

To investigate DNA and protein protection by the formation of DNA–Dps complexes, two different assays were performed.

Protection of Dps against protease degradation

To test if Dps was protected against proteolysis when bound to DNA, the DNA–protein complex was digested with Proteinase K (NZYTech), a serine protease with a broad substrate specificity. As expected, most of the protein was hydrolyzed when *M. hydrocarbonoclasticus* Dps was incubated with Proteinase K, (Fig. 7a, lane 8 and Fig. 7b, lane 12). The same result was obtained for BSA and Dps-Q14E protein (Fig. 7b, lanes 2 and 4). The incubation of the DNA–protein complex with Proteinase K (Fig. 7a, lanes 2 to 7) did not affect the complex, while the pre-incubation of Dps-WT protein with Proteinase K prevented the formation of protein–DNA complex (Fig. 7b). Staining the EMSA gels for protein detection and comparison of the intensity of Dps bands revealed that the proteolysis was less extensive on the complex, than when the free protein was incubated with the protease (bottom gels in Figure 7, lanes 2–7 on gel A versus lanes 6–11 on gel B). In the assays with Proteinase K, the Dps band presented increased mobility when compared with the free protein one, suggesting the presence of a peptide site more susceptible to proteolysis in the Dps sequence, resulting in truncated Dps molecules. This could also explain the inability of DNA binding when Dps was pre-incubated (before the DNA-binding reaction) with the protease. In fact, in the N-terminal tail (first 15 residues), there are 5 possible cleavage sites for proteinase K (in bold face in the sequence MGKN**FI**G**L**D**T** DK**T**QK).

Protection of DNA against hydroxyl radical degradation

All Dps proteins have in common the capacity to protect DNA from damage by hydroxyl radicals generated by the Fenton reaction, since they catalyze the uptake of Fe^{2+} ions and H_2O_2 from solution (ferroxidase activity). Therefore, supercoiled pUC19 was first incubated with *M. hydrocarbonoclasticus* Dps proteins (Dps-WT, Dps-Q14E and iron-loaded wild-type Dps (containing 96 Fe atoms per protein) and then exposed to an excess of Fe^{2+} ions and H_2O_2. The results are shown in Fig. 8. Supercoiled DNA was completely hydrolyzed in the presence of hydroxyl radicals (lane 2), whereas the pre-incubation with Dps proteins resulted in DNA protection (lanes 3–6). However, in the presence of Proteinase K (lane 4), DNA suffered more degradation when compared with the reaction without

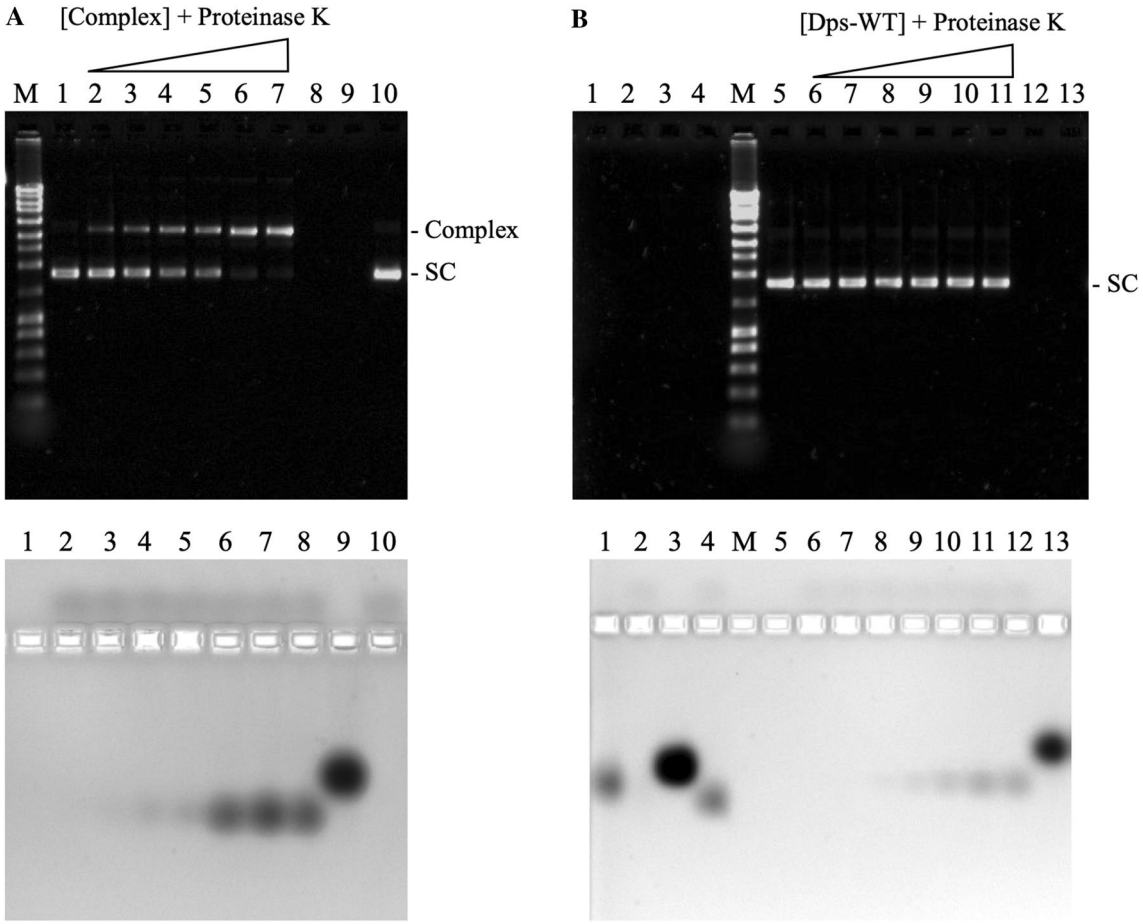

Fig. 7 Dps protein protection assays against Proteinase K. **a** DNA–protein complex incubated with Proteinase K: 1—plasmid pUC19 (10 nM); 2–7—binding reaction of Dps-WT (0.50, 1.0, 3.0, 5.0, 9.0 and 13 μM) to plasmid pUC19 (10 nM) and then incubated with Proteinase K (20 mg/mL); 8—Dps-WT (13 μM) incubated with Proteinase K; 9—Dps-WT (13 μM); 10—plasmid pUC19 (10 nM) incubated with Proteinase K. **b** Binding of Dps-WT pre-incubated with Proteinase K to supercoiled plasmid pUC19: 1—BSA protein (13 μM); 2—BSA (13 μM) incubated with Proteinase K; 3—Dps-Q14E protein (13 μM); 4—Dps-Q14E (13 μM) incubated with Proteinase K; 5—plasmid pUC19 (10 nM); 6–11—binding reaction of pre-incubated Dps-WT (0.50, 1.0, 3.0, 5.0, 9.0 and 13 μM) with Proteinase K with plasmid pUC19 (10 nM); 12—Dps-WT (13 μM) incubated with Proteinase K; 13—Dps-WT protein (13 μM). M—NZYLadder III. The free supercoiled plasmid band (SC) is indicated on the right. Upper gels stained with SYBR Safe for detection of DNA, and lower gels stained with Coomassie Brilliant Blue to detect protein

the protease (lane 3). Protection of plasmid pUC19 was still observed when pre-incubated with Dps-Q14E variant or iron-loaded Dps protein (lanes 5 and 6). Since, as demonstrated above, these two protein forms do not bind DNA (Figs. 2 and 3), the results indicate that protection of DNA was due to the ferroxidase activity (ferrous irons uptake in the presence of H_2O_2) of the Dps enzyme rather than to a physical shielding effect by protein binding.

Conclusion

The principal function of proteins from the Dps family is DNA protection, mainly through their ferroxidase activity. Besides, some Dps also have the ability to non-specifically bind DNA protecting it from oxidative damage. When present, the flexible positively charged N- or C-terminal extensions have been indicated as responsible for the interaction of Dps with DNA. *M. hydrocarbonoclasticus* Dps contains this structural element at the N-terminal extension. In this work EMSAs were performed using wild-type Dps (apo and holo forms) and a variant. A point mutation replacing glutamine-14 residue by a glutamate was introduced to infer about the importance of the N-terminal extension pI value. We do believe that this parameter is crucial for DNA binding. If the pI of the flexible N- or C-terminal extensions is not above the pKa of positive residues (lysines and arginines) DNA binding will not occur, even when these amino acid residues are present. Results confirmed our hypothesis and have shown the ability of *M. hydrocarbonoclasticus* Dps to

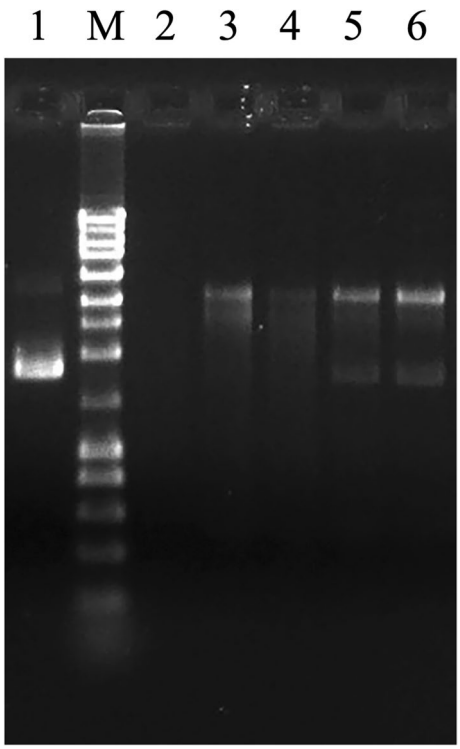

Fig. 8 Analysis of DNA protection against hydroxyl induced DNA damage. 1—plasmid pUC19 (10 nM); 2—plasmid pUC19 (10 nM) exposed to an excess of Fe^{2+} and H_2O_2; 3—Dps-WT–pUC19 complex reacted with Fe^{2+} and H_2O_2; 4—Dps-WT–pUC19 complex pre-incubated with Proteinase K and reacted with Fe^{2+} and H_2O_2; 5—Dps-Q14E variant incubated with pUC19 and then reacted with Fe^{2+} and H_2O_2; 6—iron-loaded Dps-WT (96 Fe^{2+}/protein) incubated with pUC19 and then reacted with Fe^{2+} and H_2O_2. M—NZYLadder III

bind to supercoiled plasmid DNA with a K_D of 6.0 ± 1.0 µM. Dps variant Q14E was not able to interact with DNA.

Contrarily to what was described in the literature (Ceci et al. 2007; Huergo et al. 2013), iron-loaded *M. hydrocarbonoclasticus* Dps showed no affinity to bind DNA. It is likely that the presence of Fe^{3+} ions, may affect the structure of the "ferritin-like" pores in a mechanism similar to the one proposed for mammalian fast ferritins (Tosha et al. 2012).

Formation of the protein–DNA complex proved to be important for both protein and DNA protection. Assays performed with Proteinase K demonstrated that the formation of the Dps–DNA complexes could physically shield the accessibility of the protease to the Dps molecules bound to DNA. On the other hand, protection assays against hydroxyl radicals indicated that DNA was protected due to the ferroxidase activity of the protein, since both holo-Dps-WT (containing 96 Fe per molecule) and the Dps-Q14E variant protein were still able to protect it against oxidative damage, by rapidly oxidizing Fe^{2+} ions using H_2O_2 as oxidant.

SRCD spectroscopy was used to probe the structural integrity of apo Dps-WT and holo protein, variants and protein–DNA complex. It is clear from the collected data that all protein forms retain the secondary structure characteristics expected for the Dps nanocage structure. The major difference was observed for the Dps-WT protein incubated with DNA where, while maintaining similar overall secondary structural features, a loss of α-helices components can be perceived as a perturbation upon protein–DNA complex formation. The thermal stability studies show that protein aggregation (and possible precipitation) arises above 40 °C, a behavior confirmed by DLS. This impairs the use of thermal denaturation studies to further probe structural differences between the studied proteins and protein–DNA complexes. It is, however, noteworthy to mention that the use of a periscope chamber can overcome such problem by preventing displacement effects. The smart design of a periscope chamber that places the quartz cell in a horizontal mounting position maintains the possibility of acquiring representative spectra at an extended energy range and high photon flux for protein solutions where aggregation might occur. Using this experimental setup, several SRCD experiments (in parallel with other spectroscopic and biochemical techniques) are currently being devised to understand the aggregation behavior of *M. hydrocarbonoclasticus* Dps in different experimental conditions (ionic strength, pH, crowding agents) and characterize the structural dynamics of such an interesting bionanocage system.

Supplementary Information The online version contains supplementary material available at https://doi.org/10.1007/s00249-021-01538-0.

Acknowledgements We acknowledge Professor Paulo Limão-Vieira (CEFITEC, Departamento de Física, Faculdade de Ciências e Tecnologia, Universidade Nova de Lisboa), for many insightful discussions, as well as providing help with the flux photon measurements done for the Chirascan setup.

Funding This research was supported by Fundação para a Ciência e Tecnologia, Ministério da Ciência, Tecnologia e Ensino Superior (FCT-MCTES), grant PTDC/BIA-PRO/111485/2009 (to P.T.), PTDC/QUI/64248/2006 (to A.S.P). This work was also supported by Radiation Biology and Biophysics Doctoral Training Programme (RaBBiT, PD/00193/2012, Applied Molecular Biosciences Unit–UCIBIO (UIDB/04378/2020) and CEFITEC (UIDB/00068/2020)), all financed by national funds from FCT-MCTES). J.P.J. (SFRH/BD/135056/2017), A.V.A. (PD/BD/135477/2017), J.P.L.G. (PD/BD/135476/2017) and D.P. (SFRH/BD/52535/2014) are supported by the RaBBiT programme. This work benefited from STSM funding by COST Action (CA15126 MOBIEU) and by the project CALIPSOplus under the Grant Agreement 730872 from the EU Framework Programme for Research and Innovation HORIZON 2020.

Declarations

Conflict of interest The authors declare that they have no conflict of interest.

References

Andrews SC (2010) The Ferritin-like superfamily: evolution of the biological iron storeman from a rubrerythrin-like ancestor. Biochim Biophys Acta 1800:691–705. https://doi.org/10.1016/j.bbagen.2010.05.010

Aumiller WM, Uchida M, Douglas T (2018) Protein cage assembly across multiple length scales. Chem Soc Rev 47:3433–3469. https://doi.org/10.1039/c7cs00818j

Calhoun LN, Kwon YM (2011) Structure, function and regulation of the DNA-binding protein Dps and its role in acid and oxidative stress resistance in *Escherichia coli*: a review. J Appl Microbiol 110:375–386. https://doi.org/10.1111/j.1365-2672.2010.04890.x

Ceci P (2004) DNA condensation and self-aggregation of *Escherichia coli* Dps are coupled phenomena related to the properties of the N-terminus. Nucleic Acids Res 32:5935–5944. https://doi.org/10.1093/nar/gkh915

Ceci P, Ilari A, Falvo E, Chiancone E (2003) The Dps protein of *Agrobacterium tumefaciens* does not bind to DNA but protects it toward oxidative cleavage. X-ray crystal structure, iron binding, and hydroxyl-radical scavenging properties. J Biol Chem 278:20319–20326. https://doi.org/10.1074/jbc.M302114200

Ceci P, Mangiarotti L, Rivetti C, Chiancone E (2007) The neutrophil-activating Dps protein of *Helicobacter pylori,* HP-NAP, adopts a mechanism different from *Escherichia coli* Dps to bind and condense DNA. Nucleic Acids Res 35:2247–2256. https://doi.org/10.1093/nar/gkm077

Chiancone E, Ceci P (2010) The multifaceted capacity of Dps proteins to combat bacterial stress conditions: detoxification of iron and hydrogen peroxide and DNA binding. Biochim Biophys Acta 1800:798–805. https://doi.org/10.1016/j.bbagen.2010.01.013

Crichton R (2002) Intracellular iron storage and biomineralization. In: Inorganic biochemistry of iron metabolism. Wiley, pp 133–165

Crichton RR, Declercq J-P (2010) X-ray structures of ferritins and related proteins. Biochim Biophys Acta 1800:706–718. https://doi.org/10.1016/j.bbagen.2010.03.019

de Alcântara NR, de Oliveira FM, Garcia W et al (2020) Dps protein is related to resistance of *Mycobacterium abscessus* subsp. *massiliense* against stressful conditions. Appl Microbiol Biotechnol 104:5065–5080. https://doi.org/10.1007/s00253-020-10586-z

Grant RA, Filman DJ, Finkel SE et al (1998) The crystal structure of Dps, a ferritin homolog that binds and protects DNA. Nat Struct Biol 5:294–303. https://doi.org/10.1038/nsb0698-432

Haikarainen T, Papageorgiou AC (2010) Dps-like proteins: structural and functional insights into a versatile protein family. Cell Mol Life Sci 67:341–351. https://doi.org/10.1007/s00018-009-0168-2

Heddle JG, Chakraborti S, Iwasaki K (2017) Natural and artificial protein cages: design, structure and therapeutic applications. Curr Opin Struct Biol 43:148–155. https://doi.org/10.1016/j.sbi.2017.03.007

Hitchings MD, Townsend P, Pohl E et al (2014) A tale of tails: deciphering the contribution of terminal tails to the biochemical properties of two Dps proteins from *Streptomyces coelicolor*. Cell Mol Life Sci 71:4911–4926. https://doi.org/10.1007/s00018-014-1658-4

Huergo LF, Rahman H, Ibrahimovic A et al (2013) *Campylobacter jejuni* Dps protein binds DNA in the presence of iron or hydrogen peroxide. J Bacteriol 195:1970–1978. https://doi.org/10.1128/JB.00059-13

Ilari A, Stefanini S, Chiancone E, Tsernoglou D (2000) The dodecameric ferritin from *Listeria innocua* contains a novel intersubunit iron-binding site. Nat Struct Biol 7:38–43. https://doi.org/10.1038/71236

Janissen R, Arens MMA, Vtyurina NN et al (2018) Global DNA compaction in stationary-phase bacteria does not affect transcription. Cell 174:1188-1199.e14. https://doi.org/10.1016/j.cell.2018.06.049

Karas VO, Westerlaken I, Meyer AS (2015) The DNA-binding protein from starved cells (Dps) utilizes dual functions to defend cells against multiple stresses. J Bacteriol 197:3206–3215. https://doi.org/10.1128/JB.00475-15

Moparthi VK, Moparthi SB, Howe C et al (2019) Structural diffusion properties of two atypical Dps from the cyanobacterium Nostoc punctiforme disclose interactions with ferredoxins and DNA. Biochim Biophys Acta 1860:148063. https://doi.org/10.1016/j.bbabio.2019.148063

Nair S, Finkel SE (2004) Dps protects cells against multiple stresses during stationary phase. J Bacteriol 186:4192–4198. https://doi.org/10.1128/JB.186.13.4192-4198.2004

Nguyen KH, Smith LT, Xiao L et al (2012) On the stoichiometry of *Deinococcus radiodurans* Dps-1 binding to duplex DNA. Proteins Struct Funct Bioinform 80:713–721. https://doi.org/10.1002/prot.23228

Paszko E, Senge MO (2012) Immunoliposomes. Curr Med Chem 19:5239–5277. https://doi.org/10.2174/092986712803833362

Penas D, Pereira AS, Tavares P (2019) Direct evidence for ferrous ion oxidation and incorporation in the absence of oxidants by Dps from *Marinobacter hydrocarbonoclasticus*. Angew Chemie 58:1013–1018. https://doi.org/10.1002/anie.201809584

Pesek J, Büchler R, Albrecht R et al (2011) Structure and mechanism of iron translocation by a Dps protein from *Microbacterium arborescens*. J Biol Chem 286:34872–34882. https://doi.org/10.1074/jbc.M111.246108

Stillman TJ, Upadhyay M, Norte VA et al (2005) The crystal structures of *Lactococcus lactis* MG1363 Dps proteins reveal the presence of an N-terminal helix that is required for DNA binding. Mol Microbiol 57:1101–1112

Theil EC, Tosha T, Behera RK (2016) Solving biology's iron chemistry problem with ferritin protein nanocages. Acc Chem Res 49:784–791. https://doi.org/10.1021/ar500469e

Timóteo CG, Guilherme M, Penas D et al (2012) *Desulfovibrio vulgaris* bacterioferritin uses H_2O_2 as a co-substrate for iron oxidation and reveals DPS-like DNA protection and binding activities. Biochem J 446:125–133. https://doi.org/10.1042/BJ20111439

Tosha T, Behera RK, Ng H-L et al (2012) Ferritin protein nanocage ion channels. J Biol Chem 287:13016–13025. https://doi.org/10.1074/jbc.M111.332734

Wolf SG, Frenkiel D, Arad T et al (1999) DNA protection by stress-induced biocrystallization. Nature 400:83–85. https://doi.org/10.1038/21918

Zeth K (2012) Dps biomineralizing proteins: multifunctional architects of nature. Biochem J 445:297–311. https://doi.org/10.1042/BJ20120514

Zhang Y, Orner BP (2011) Self-Assembly in the ferritin nano-cage protein superfamily. Int J Mol Sci 12:5406–5421. https://doi.org/10.3390/ijms12085406